https://doi.org/10.48048/tis.2022.4642

Corrosion Behavior of AISI 316L Stainless Steel in a Highly Sour Environment

Mazlan Shah[1,2], Najmiddin Yaakob[3], Muhammad Taqiyuddin Mawardi Ayob[1] and Norinsan Kamil Othman[3,*]

[1]DNV Malaysia Sdn. Bhd., Level 18, Menara Prestige, Kuala Lumpur, Malaysia
[2]Department of Applied Physics, Faculty of Science and Technology, The National University of Malaysia, Selangor, Malaysia
[3]Center of Industrial Process Reliability and Sustainability, Faculty of Chemical Engineering, Universiti Teknologi MARA, Selangor, Malaysia

([*]Corresponding author's e-mail: insan@ukm.edu.my)

Received: 21 May 2021, Revised: 21 June 2021, Accepted: 28 June 2021

Abstract

Sour corrosion in the presence of H_2S gases can significantly affect the passive films deterioration of the 316L steel. 0 and 3 bar of H_2S gases were chosen to identify how H_2S gases could affect the corrosion rate on steels surface at normal and extremely sour conditions. Experiment was operated in an 7L autoclave for 7 days and was kept at 60 °C throughout the testing. The uniform corrosion rates were measured by weight loss while the pitting corrosion rates were determined by using a profilometer, respectively. The oxide layers formed under these conditions were determined by XPS. The results found that at 3 bar of H_2S gas condition shows the formation of multi-layers consist of Fe_3O_4, $(NiOH)_2$, NiO, MoO_3, FeS, and NiS. Finally, corrosion products formation on 316L steels surface was then discussed.

Keywords: Sour corrosion, Localized corrosion, Partial pressure of H_2S, 316L Stainless-steel, Passive film

Introduction

The corrosion-resistant alloy (CRA) has been introduced to the pipeline industry due to its excellent properties of corrosion resistance to survive in extreme working conditions [1]. However, the corrosion behavior of CRA in a highly sour environment still remains unclear and needs to be further investigated. One of the basis corrosion mechanisms is hydrogen embrittlement effect in the presence of H_2S, leading to localized corrosion and/or sulfide stress cracking (SSC) [2]. There are several types of CRAs such as nickel-based alloys, duplex steel, martensitic steel, and austenitic steel [3]. CRAs, such as austenitic stainless steel, shows great corrosion resistance with the formation of passive films on the steels surface in working conditions [4]. This passive film acts as a shield to protect the metal from the corrosive environment [5,6].

Stainless-steel type 316L is widely used for piping in the oil and gas industries [7]. The 316L steel is one of the austenitic alloys containing chromium, nickel and molybdenum, making it more corrosion resistant. Hesketh *et al.* [8] reported on the corrosion resistance of stainless-steel type 316L in a simulated oilfield environment to identified the H_2S gas pressure affected on physical dan chemical properties of steels samples. They found that pitting corrosion was most significant at intermediate of H_2S gas pressure, compared to free H_2S and higher H_2S gas pressure. In addition, the effect of chromium and nickel content in metals also affected the passive films formation and deterioaration [6]. Besides, there are multiple types of passive film which were formed at various parameter conditions, primarily consisting of Cr_2O_3, $Cr(OH)_3$, FeOOH, Fe_2O_3, Fe_3O_4, MoO_3 and MoO_2.

The corrosion behavior of 316L in a simulated formation of water environment with ammonium chloride (NH_4Cl) and sodium thiosulfate ($Na_2S_2O_3$) mixed solution, with different electrochemical measurements, has been studied by Al-Mamun *et al.* [9]. They demonstrated that 316L sample was improved metastable pitting resistance in the presence of $S_2O_3^{2-}$ into Cl^- solution. At high concentrations of $S_2O_3^{2-}$, the diffusion of sulfur into the oxide film was accelerated due to local breakdown of the oxide materials, leading to the formation of metal sulfides. Qiu's report proved a negative effect of SO_4^{2-} in

molten FLiNaK salt on the stability of the oxide layer of austenitic steel, which leads to less protection for the metal [10].

Due to high amount of sulfur present in the crude oil, which defects in oil and gas infrastructure (e.g., pipelines and processing plant), this work investigates the effects of H_2S gas pressure on the AISI 316L stainless-steel, with the emphasis on the formation and deterioration of passive films. The relationship between the parameter conditions and the develops of the corrosion product layers on the steel surface are discussed.

Materials and methods

The austenitic stainless-steel grade AISI 316L specimens were cut into a dimension of 20×20×3 mm^3 (width×length×high) using a laser cutter. Prior to each experiment, the weight loss of 316L steels were polished using silicon carbide abrasive papers (up to 1,200 grit) and isopropyl alcohol as a coolant. The chemical composition of the 316L steels sample was tested using optical emission vacuum spectrometer to analyses the AISI 316L steel following ASTM E 1086 standard through the point-to-plane excitation technique as shown in **Table 1**.

Table 1 The chemical composition of tested AISI 316L steel (wt.%).

C	Mn	Si	P	S	Mo	Cr	Cu	Al	Fe
0.02	1.31	0.43	0.03	0.01	2.08	16.48	0.34	0.01	Bal.

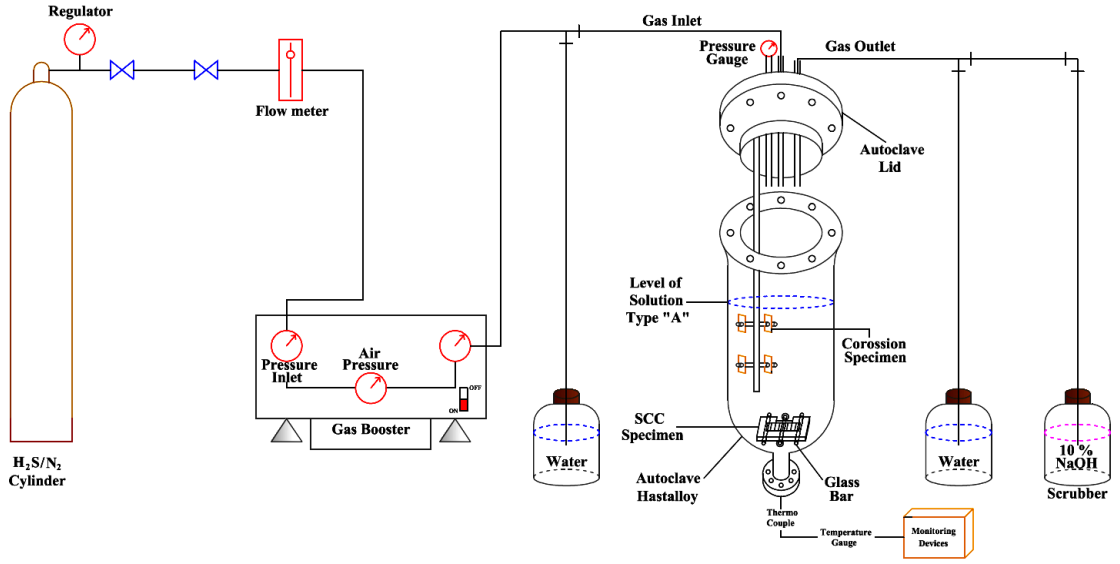

Figure 1 Schematic diagram of the autoclave system.

Experiments were operated in a 7L autoclave (UNS N10276 Hastelloy), which enabled it to withstand the high pressure and temperature for 7 days, as shown in **Figure 1**. The experimental conditions were set at a total pressure of 30 bar with 3 and 27 bar partial pressures of H_2S and N_2 gases, respectively and maintained at 60 °C throughout the experiment. The 316L steel was immersed in NACE TM0177 Solution-A, which consisting of mixed 0.5 wt.% CH_3COOH, 5 wt.% NaCl and distilled water. Experimental was repeated with 0 bar H_2S gas as control coupon and 3 bar H_2S gas was chosen for parameter study represent a majority industry field and within a limit for material in highly sour condition as stated in ANSI/NACE MR0175/ISO 15156-3: 2015(E). Before the beginning of each test, 5L of distilled water were added to the autoclave and deoxygenated process for 2 h has been done to remove residual oxygen from the test solution when the oxygen content is higher than required. The 316L steel samples were mounted in the specimen holder by a customized Polytetrafluoroethylene (PTFE) washer,

bush and nut, to ensure that the specimen with its holder was electrically isolated. The holder was then mounted to the autoclave cover, as shown in **Figure 2**.

At the end of the experiment, the gas phase was purged for 2 h with nitrogen gas before demounting the products from the autoclave. The products were rinsed 3 times with isopropanol, dried and weighed. Transmission Electron Microscope (TEM), Scanning electron microscopy (SEM) with electron dispersive X-ray spectroscopy (EDS) and X-ray photoelectron spectroscopy (XPS) analyses were performed for surface analysis prior to weight loss determination, according to ASTM G1-03 standard, [11] which is to calculated the corrosion rate and identified the corrosion products formed on the 316L steel sample. After that, surface profile analysis was accomplished to examine the pitting corrosion by measuring the pit depth using a profilometer. All of the test matrix values for the work are shown in **Table 2**.

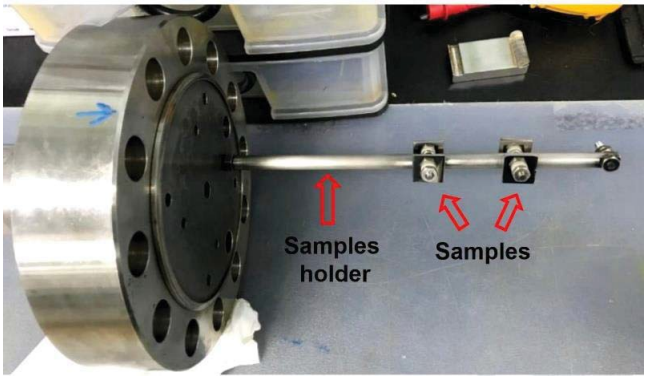

Figure 2 Autoclave lid with sample holder.

Table 2 Test matrix.

Investigating corrosion behavior	**With H_2S**	**Without H_2S**
Test Material	AISI 316L Stainless-steel	
Total pressure (Bar)	30	
Liquid Temperature (°C)	60	
Measured pH	2.63	3.42
Pressure H_2S (Bar)	3	0
Pressure N_2 (Bar)	27	30
Test duration (hour)	168	
Solution	NACE TM0177 Solution A	

Results and discussion

Corrosion rate analysis

The uniform and pit corrosion rate of 316L steels sample for both conditions at 0 and 3 bar H_2S gases were obtained from weight loss calculation and measurement of the deepest pit from profilometry analysis (IFM), which is in accordance with ASTM G 46-9411 as shown in **Figures 3** and **4**. From **Figure 3**, the uniform corrosion rate was significantly increased by tenfold from 0.07 ± 0.01 mm/yr (0 bar H_2S gas) to 0.7 ± .0.03 mm/yr (3 bar H_2S gas), respectively. In addition, the deepest pit value at 46.81 µm, was measured at 3 bar H_2S gas with a pit penetration rate of 2.4 mm/yr, as compared to that of only 3.34 µm pit depth and 0.17 mm/yr pit penetration rate at 0 bar H_2S gas. It can be clearly seen that the presence of 3 bar of H_2S gas accelerates both the uniform and pit penetration. Therefore, the corrosion resistance on the 316L steels surface seem diminished and the corrosion product layer became thicker [8].

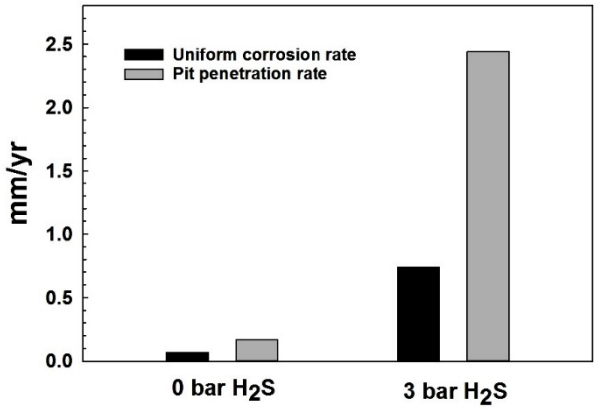

Figure 3 Comparison of uniform corrosion rate and pit penetration rate for 316L stainless steel samples with 0 and 3 bar partial pressure of H_2S gas at 60 °C.

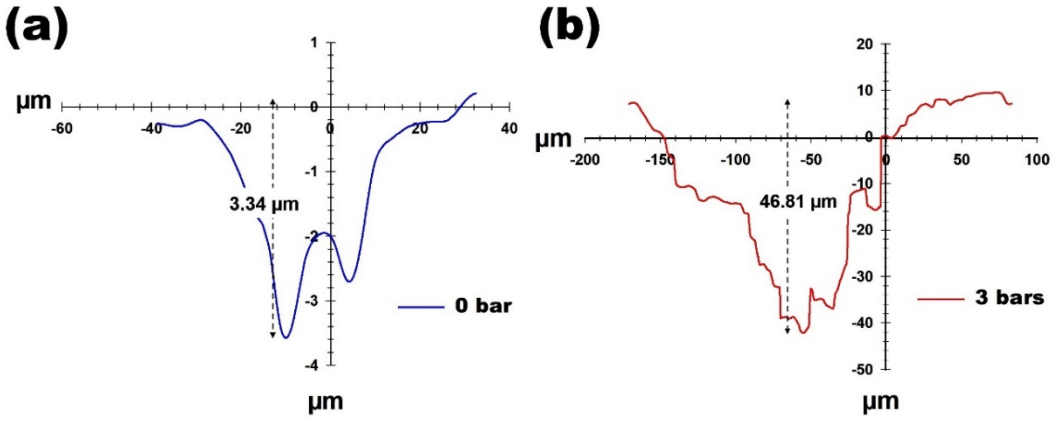

Figure 4 Deepest pits formation on 316L steels at (a) 0 bar H_2S gas and (b) 3 bar H_2S gas conditions.

Surface morphology of 316L stainless-steel

The surface morphology of the 316L steels for both conditions (0 and 3 bar H_2S gases) were analysed using SEM instrument as shown in **Figure 5**. At 0 bar of H_2S gas, there was no effect of localized corrosion as the metal surface was covered by a thin passive layer, however the steel polishing marks could still be seen, as shown in **Figure 5(a)**. Based on the EDX analysis, the most probable passive layer formed is a chromium oxide layer at final experiment, and this result has been supported by XPS analysis as shown in **Table 3**. However, **Figure 5(b)** shows the local breakdown of the oxide layer was observed due to sulfide initiator which could possibly lead to pitting corrosion underneath the layer at 3 bar H_2S gas condition. Monnot *et al*. [12] also observed that the thickness of the oxide layer was not uniform and line cracking were found on the steels surface after immersion in NACE solution-B, with the mixed of 10 % H_2S and 90 % CO_2 gases. Besides, the EDX analysis shows Ni, Fe, and S compounds were identified on 316L steel at 3 bar H_2S conditions. The wt.% of Cr content in the passive film area is reduced when compared to 0 bar H_2S gas conditions due to dissolution of Cr compound in the test solution.

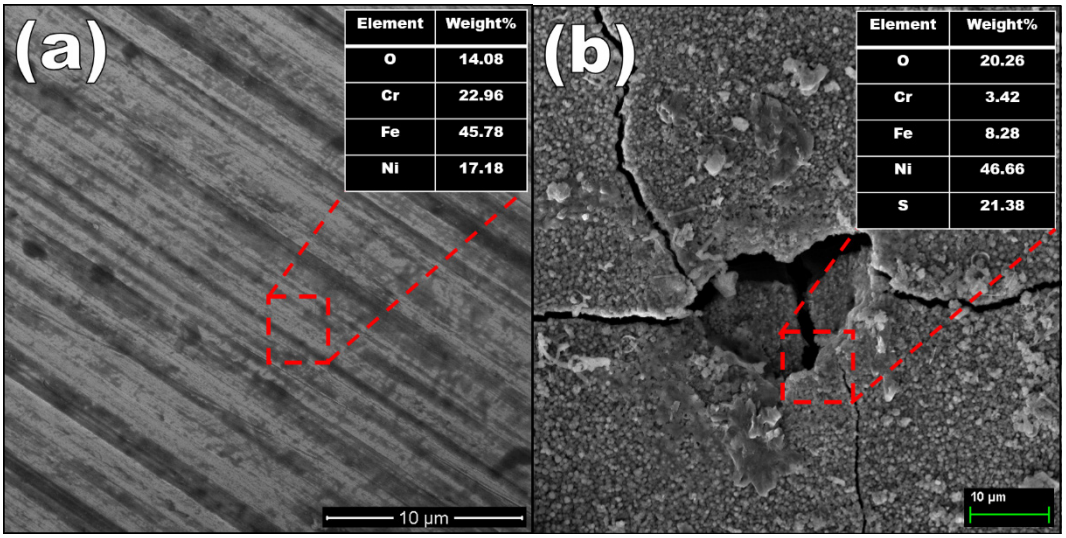

Figure 5 Morphology images of 316L steels surface at (a) 0 bar H_2S gas and (b) 3 bar H_2S gas conditions.

The corrosion products formed on the 316L steels at different H_2S gases conditions was investigated to identified the deterioration of the 316L steels surface. The comparison of the XPS results from both conditions can provide information on the corrosion products formation, as shown in **Figures 6 - 8**. Thus, **Figure 6** displays the high-resolution spectra for (a) Cr 2p and (b) Mo 3d, recorded on the 316L steels sample exposed at 0 bar H_2S gas condition. The Cr 2p narrow spectra in **Figure 6(a)** consists of 3 constituent peaks at different binding energies attributed to $Cr(OH)_3$ (577.03 eV), Cr_2O_3 (578.48 eV), and CrO_3 (587.23 eV), respectively. $Cr(OH)_3$ is the primary chromium species that was observed after the analysis due to highest and broad peak as shown in **Figure 6(a)**. On the contrary, **Figure 6(b)** demonstrates the Mo 3d spectra that attained from the 316L steels sample at 0 bar H_2S gas condition. The curve fitting shows that the 4 peaks at 232.96, 232.21, 232.86 and 237.34 eV are attributed to Mo, MoO_2, MoO_4 and MoO_3, respectively.[13] Therefore, the passive film developed at 0 bar H_2S gas condition mainly comprises of $Cr(OH)_3$, CrO_3, Cr_2O_3, MoO_2, MoO_4 and MoO_3.

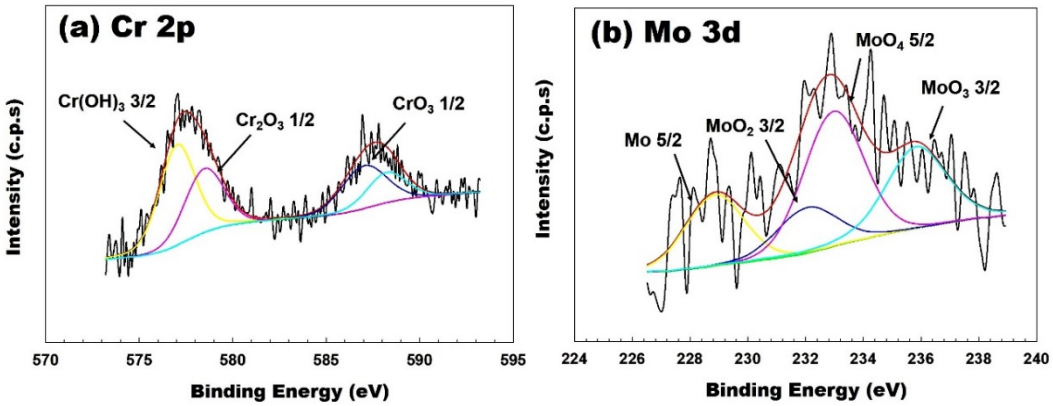

Figure 6 The deconvolution spectra of corrosion products developed on 316L stainless steels surface with a narrow scan of (a) Cr 2p and (b) Mo 3d at 0 bar H_2S gas condition.

Figure 7 shows the elemental contribution analysis for S 2p, Mo 3d, Ni 2p and Fe 2p, recorded at final experiment. The Cr element was not detected in the passive film due to its instability in the environmental conditions, as discussed in the FESEM section (**Figure 5**). The Ni 2p narrow spectra is fitted to 3 peaks, which are $Ni(OH)_2$ ($2p_{3/2}$:857.8 eV & $2p_{1/2}$:875.7 eV), NiO ($2p_{3/2}$:856.2 eV & $2p_{1/2}$:874.3 eV) and NiS ($2p_{3/2}$:854.1 eV & $2p_{1/2}$:872.5 eV) as shown in **Figure 7(a)**. 2 satellite peaks also appear at

861.7 and 880 eV in the spectra. The existence of NiS compound in the passive film is due to the excessive of ionic sulfide and depletion of the Mo element in the oxide layer. Apart from that, Monteiro *et al*. [14] have reported that traces of $Ni(OH)_2$ and NiO compounds also being distinguished in the passive film. **Figure 7(b)** shows the XPS spectra of Fe 2p obtained at 3 bar H_2S gas condition. There are 2 major peaks in the Fe 2p spectra which attributed to Fe_3O_4 (710.1 eV) and FeS (712.7 eV) compounds. The FeS species was formed from the reaction between Fe and S elements, indicating the sulfidation occurred on the steels surface. Apart from that, the Mo spectra exhibited 2 component peaks of Mo 3d 5/2 which are attributed to MoO_3 ($3d_{5/2}$:232.6 eV) and Mo metallic ($3d_{5/2}$:226.82 eV), with satellite peaks (230 & 235.6 eV), as shown in **Figure 7(c)**. Other than Mo, the S 2p spectra of the 316L steels surfaces was dominated by FeS_2 ($2p_{3/4}$:162.3 eV & $2p_{1/2}$:163.8 eV) and NiS ($2p_{3/4}$:162.9 eV & $2p_{1/2}$:164.8 eV) compounds, as shown in **Figure 7(d)**. Zhang *et al*. [15] reported similar findings where NiS and FeS_2 were present on 316L steel after immersion at 120 °C, 1 bar H_2S, 5 bar CO_2 and 130 K mgL^{-1} chloride conditions for 30 days. However, there are no chromium sulfide and molybdenum sulfide present in **Figure 7(d)** due to its dissolution into solution and the Mo was insufficient to react with sulfur.

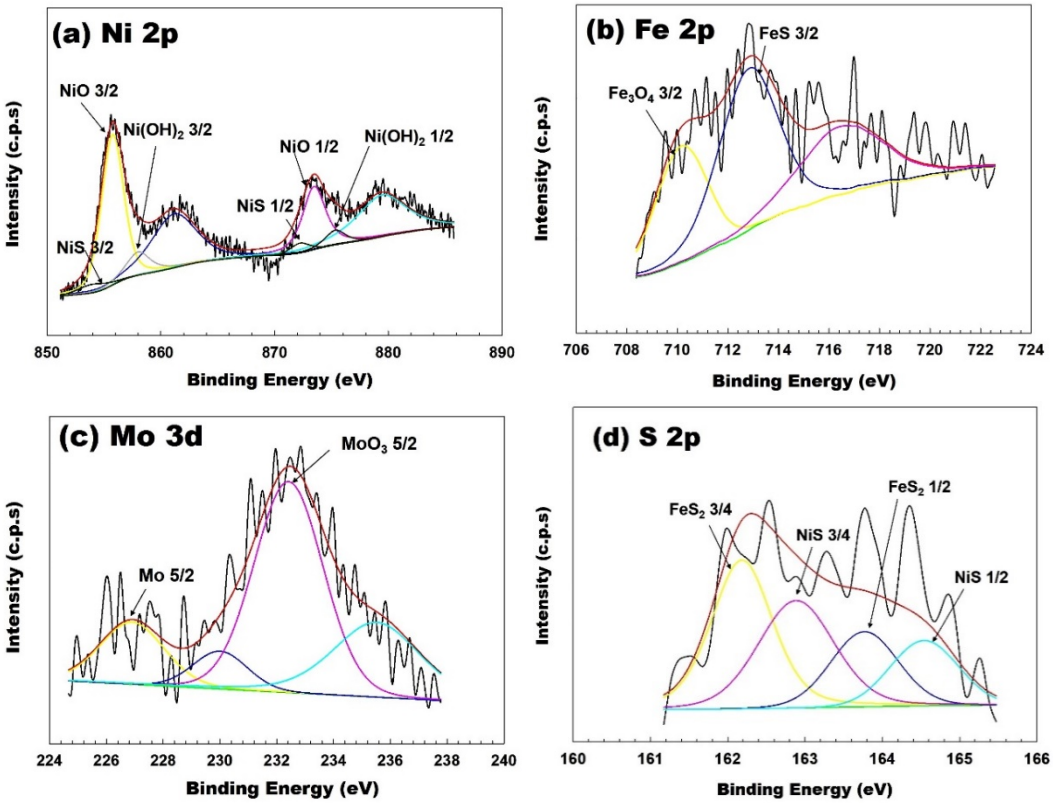

Figure 7 The deconvolution spectra of corrosion products developed on 316L stainless steels surface with a narrow scan of a) Ni 2p, (b) Fe 2p, (c) Mo 3d and (d) S 2p at 3 bar H_2S gas condition.

Figure 8 shows the narrow scan of O 1s spectra for 316L steels for both 0 bar and 3 bar H_2S gases conditions. **Figure 8(a)** shows the O 1s spectra at 0 bar H_2S gas condition which fitted for 2 component peaks, attributed to MoO_3 (530.6 eV) and Cr_2O_3 (531.9 eV) compounds. Cr_2O_3 seems the primary oxide species that was produced in the 0 bar H_2S gas condition. However, the O 1s spectra in 3 bar H_2S gas presence are decomposed into 4 component peaks which dominated by NiO (529.4 eV), MoO_3 (530.7 eV), Fe_3O_4 (531.6 eV) and $Ni(OH)_2$ (532.5 eV), as shown in **Figure 8(b)**. Fe_3O_4 compound had the highest atomic concentration of the oxide species, indicating that it was the main compound present in the passive films at highly sour conditions. Consequently, the passive film turns into a non-protective film formed at 3 bar H_2S. The disappearance of Cr layer is due to the instability of the passive layer when exposed to a highly sour environment due to passive film degradation [16].

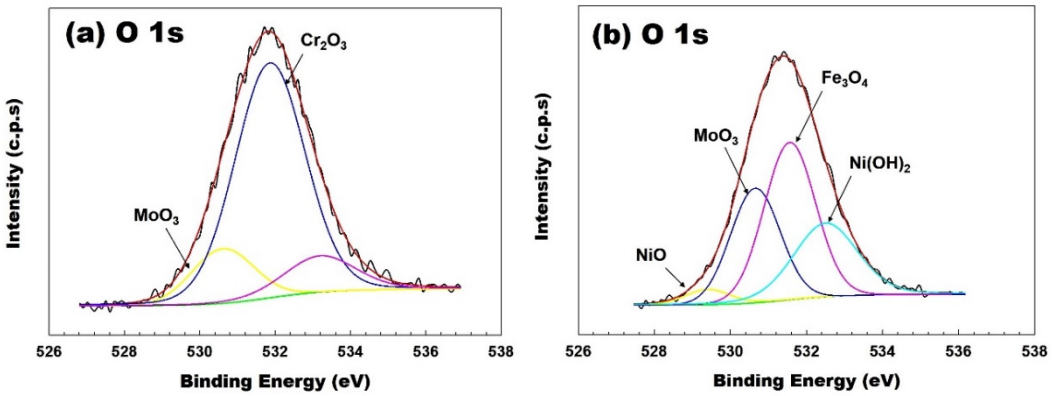

Figure 8 The deconvolution spectra of corrosion products developed on 316L stainless steels surface with a narrow scan of O 1s at (a) 0 bar H_2S gas and (b) 3 bar H_2S gas conditions.

Lateral cross-section analysis (FIB/TEM)

TEM analysis with FIB preparation samples was conducted to investigate the corrosion layer of 316L steels samples at 3 bar H_2S condition. The procedure involves the dividing of a thin material around the substrate/passive layer via FIB instrument. The subsequent microscopic and elemental analysis of samples were done using TEM and EDS, respectively. The 4 areas marked by red circles, named as point 1 until point 4, were analyzed by TEM (**Figure 9(a)**) and EDS (**Figure 9(b)**). Some elements such as Fe, S, O, Mo and Ni were identified from the passive films in both conditions, and the existence of Fe reveals that the ionic sulfide has penetrated into the passive film/substrate interface and caused the deterioration of the 316L steel substrate.

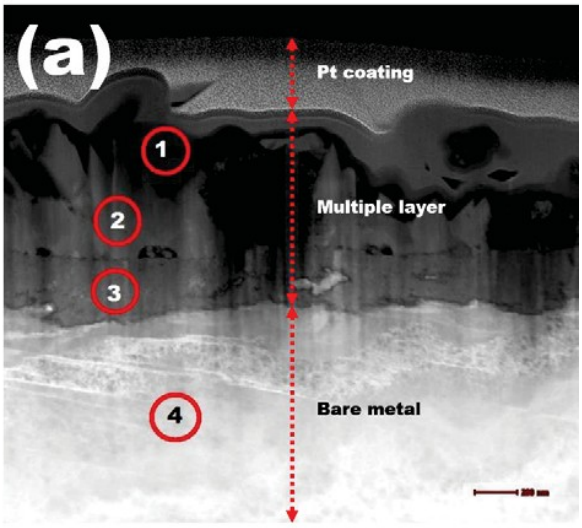

(b)

Element	Point (wt%) 1	2	3	4
O	19.73	8.71	9.77	7.59
Ni	19.62	51.42	53.43	13.18
Fe	20.93	8.95	11.14	74.07
S	19.98	22.54	25.66	5.16
Mo	19.83	8.38	-	-

Figure 9 (a) The cross-section image of passive film formed at 3 bar H_2S gas with point EDS marked and (b) Point EDS results. Scale bar: 200 nm.

From the chemical compositions in EDS points 1 and 2, the Mo element was detected. However, the weight percent of Mo at point 1 is higher than that at point 2 due to the difference of position/layer of the thin film. The EDS point 1 position seems to be in the outer layer of the thin slice sample substrate. Thus, the Mo element that contributes in point 1 was MoO_3, as referred to the XPS results. The EDS point 2 and 3 positions seem to be in the inner layer of the thin film substrate. Besides, S, O, Ni and Fe, elements without Mo are detected at point 3 and 4 due to a mixture of Ni-, Fe- oxide and sulfide. The primary elements that were found at this area are NiS, NiO, $Ni(OH)_2$, Fe_3O_4, FeS_2 and FeS. Besides, the wt.% of

NiS compound seems higher at point 3 regarding the Ni enrichment of about 53.43 wt.%, as mentioned in **Figure 9(b)**. The enrichment of Ni has also been reported in the literature [17]. From EDS point 4, the Fe element is enriched by about 74 %, which corresponds to the bare metal. As the scan progressed through the EDS points, it can be concluded that the outer layer was made of Mo signal, which was mainly formed of MoO_3, and the inner layer consists of Ni-, Fe-oxides and sulfides. Therefore, the multiple oxide layers that were formed consist of NiS, NiO, $Ni(OH)_2$, FeS_{24}, FeS and Fe_3O. Similarly, Wang *et al*. [16] also found that the multiple oxide layers formed at several pH values from pH 3 to pH 6 were mainly composed of Cr_2O_3, $Cr(OH)_3$, FeS, $Fe(OH)_2$, Fe_2O_3 and NiO on 316L steels surface in a conditions under H_2S/N_2 gases with mole ratio of $H_2S:N_2$ = 1:9. This result is in agreement with our findings except for the chromium element. **Figure 10** depicts the cross-sectional images of the multiple layers on the 316L steels at 3 bar H_2S gas condition with a nano-porous network consisting of an amorphous/non-crystalline form of corrosion products.

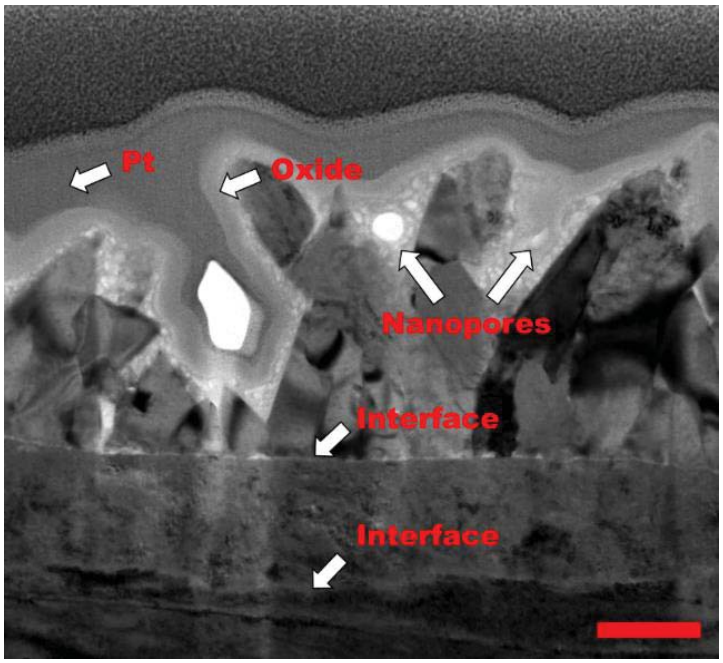

Figure 10 Cross-sectional morphology of the passive film developed on the 316L stainless-steel after exposed to 3 bar H_2S gas. Scale bar: 200 nm

Conclusions

The comparison of the passive film deterioration for 316L stainless steel on both 0 and 3 bar H_2S gases has been studied using NACE solution-A medium. The key findings from this study are summarized as follows:

1) Pit penetration rate was increased from 0.17 mm/yr (0 bar) to 2.4 mm/yr (3 bar). Meanwhile, uniform corrosion rate also increased from 0.07 mm/yr (0 bar) to 0.7 mm/yr (3 bar) for 316L stainless steel, when exposed to 3 bar H_2S gas condition.

2) At 0 bar of H_2S gas, there was no effect of localized corrosion as the metal surface was covered by a thin passive layer. However, the local breakdown of the oxide layer was observed due to sulfide initiator which could possibly lead to pitting corrosion underneath the layer at 3 bar H_2S gas condition.

3) At 0 bar H_2S gas, very thin Chromium (CrO_3, Cr_2O_3) and Molybdenum (MoO_2, MoO_3) based protective oxide layers were formed. However, multiple non-protective oxide layers were formed at 3 bar of H_2S gas which consisted of $Ni(OH)_2$, NiO, NiS, Mo, MoO_3, Fe_3O_4, and FeS.

Acknowledgements

We would like to express our appreciation to DNV Malaysia Sdn. Bhd. and The National University of Malaysia for financial and facilities support.

References

[1] RB Rebak and TE Perez. Effect of carbon dioxide and hydrogen sulfide on the localized corrosion of carbon steels and corrosion resistant alloys. *In*: Proceedings of the NACE International Corrosion 2017 Conference, Texas, United States. 2017, p. 1-15.

[2] J Kvarekvål and J Moloney. *Sour corrosion. In*: AM El-Sherik (Ed.). *Trends in oil and gas corrosion research and technologies*: *Production and transmission*, Woodhead Publishing, Sawston, United Kingdom, 2017, p. 113-42.

[3] M Muhammed, M Mustapha, TL Ginta, AM Ali, F Mustapha and CC Hampo. Statistical review of microstructure-property correlation of stainless steel: Implication for pre-and post-weld treatment. *Processes* 2020; **8**, 811.

[4] MA Rao, RS Babu and MV Pavan Kumar. Stress corrosion cracking failure of a SS 316L high pressure heater tube. *Eng. Fail. Anal.* 2018; **90**, 14-22.

[5] M Liu, S Bell, M Segarra, NH Steven, G Will, W Saman and F Bruno. A eutectic salt high temperature phase change material: Thermal stability and corrosion of SS316 with respect to thermal cycling. *Sol. Energ. Mater. Sol. Cell.* 2017; **170**, 1-7.

[6] S Zhang, C Sun, J Di and Y Tan. Corrosion behavior and morphology of passive films modified with zinc-aluminum simultaneous treatment on different metals. *Materials* 2020; **10**, 986.

[7] D Li, Q Liu, W Wang, L Jin and H Xiao. Corrosion behavior of AISI 316L stainless steel used as inner lining of bimetallic pipe in a seawater environment. *Materials* 2021; **14**, 1539.

[8] J Hesketh, EJF Dickinson, ML Martin, G Hinds and A Turnbull. Influence of H_2S on the pitting corrosion of 316L stainless steel in oilfield brine. *Corrosion Sci.* 2021; **182**, 109265.

[9] NS Al-Mamun, W Haider and I Shabib. Corrosion resistance of additively manufactured 316L stainless steel in chloride-thiosulfate environment. *Electrochim. Acta* 2020; **362**, 137039.

[10] J Qiu, B Leng, H Liu, DD Macdonald, A Wu, Y Jia, W Xue, G Yu and X Zhou. Effect of SO_4^{2-} on the corrosion of 316L stainless steel in molten FLiNaK salt. *Corrosion Sci.* 2018; **144**, 224-9.

[11] ASTM International. *Standard practice for preparing, cleaning, and evaluating corrosion test specimens.* ASTM International, Pennsylvania, United States, 2017.

[12] M Monnot, RP Nogueira, V Roche, G Berthomé, E Chauveau, R Estevez and M Mantel. Sulfide stress corrosion study of a super martensitic stainless steel in H_2S sour environments: Metallic sulfides formation and hydrogen embrittlement. *Appl. Surf. Sci.* 2017; **394**, 132-41.

[13] M Shah, MTM Ayob, R Rosdan, N Yaakob, Z Embong and NK Othman. The effect of H_2S pressure on the formation of multiple corrosion products on 316L stainless steel surface. *Sci. World J.* **2020**; 2020, 3989563.

[14] RD Monteiro, JVD Wetering, B Krawczyk and DL Engelberg. Corrosion behaviour of type 316L stainless steel in hot caustic aqueous environments. *Met. Mater. Int.* 2020; **26**, 630-40.

[15] L Zhang, X Tang, Z Wang, T Li, Z Zhang and M Lu. The corrosion behavior of 316L stainless steel in H2S environment at high temperatures. *Int. J. Electrochem. Sci*. 2017; **12**, 8806-19.

[16] Z Wang, L Zhang, Z Zhang and M Lu. Combined effect of pH and H_2S on the structure of passive film formed on type 316L stainless steel. *Appl. Surf. Sci.* 2018; **458**, 686-99.

[17] KL Cwalina, HM Ha, N Ott, P Reinke, N Birbilis and JR Scully. In operando analysis of passive film growth on Ni-Cr and Ni-Cr-Mo alloys in chloride solutions. *J. Electrochem. Soc.* 2019; **166**, 3241-52.